Electronic Supplementary Material (ESI) for Dalton Transactions.

Electronic Supporting Materials

Molecular iodine adsorption within the Hofmann-type structures M(L)[M'(CN)$_4$] (M = Ni, Co; M' = Ni, Pd, Pt): impact of their composition.

Giovanni Massasso,[†] Maria Rodriguez-Castillo,[†] Jérôme Long,[†] Julien Haines,[†] Sabine Devautour-Vinot,[†] Guillaume Maurin,[†] Agnès Grandjean,[‡] Barbara Onida,[§] Bruno Donnadieu,[#] Joulia Larionova,[†] * Christian Guérin[†] and Yannick Guari[†]

[†] *Institut Charles Gerhardt Montpellier, UMR 5253, CNRS-UM2-ENSCM-UM1, IMNO (G. M., J. Lo, C. G., Y. G. J. La), C2M (J. H.), DAMP (S. D.-V., G. M.). Université de Montpellier, Place E. Bataillon, 34095, Montpellier, France.*

[‡] *CEA/DEN/DTCD/SPDE, Laboratoire des Procédés Supercritiques et de Décontamination, BP 17171, 30207 Bagnols sur Cèze, France.*

[§] *Institute of Chemistry, Department of Applied Science and Technology, Politecnico di Torino, Corso Duca degli Abruzzi 24, 10129 Torino, Italy.*

[#] *Fédération de Recherche Chimie Balard- FR3105, Université de Montpellier, Place E. Bataillon, 34095 Montpellier, France.*

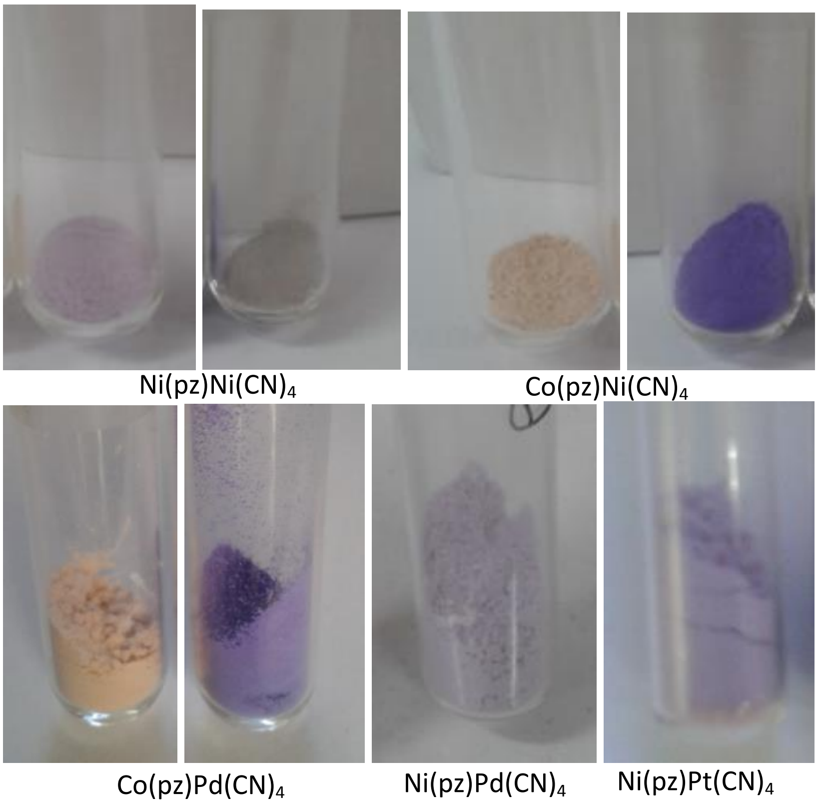
Ni(pz)Ni(CN)$_4$
Co(pz)Ni(CN)$_4$
Co(pz)Pd(CN)$_4$
Ni(pz)Pd(CN)$_4$
Ni(pz)Pt(CN)$_4$

Fig. S1. Photographs of the Hofmann clathrates powders M(pz)[M'(CN)$_4$]·2H$_2$O (M = Ni^{II}, Co^{II} and M' = Ni^{II}, Pd^{II}, Pt^{II}, pz = pyrazine) before (right) and after (left) thermal activation under vacuum at 80 °C. The compounds Ni(pz)[Pd(CN)$_4$]·2H$_2$O and Ni(pz)[Pt(CN)$_4$]·2H$_2$O don't change their color after the thermal treatment.

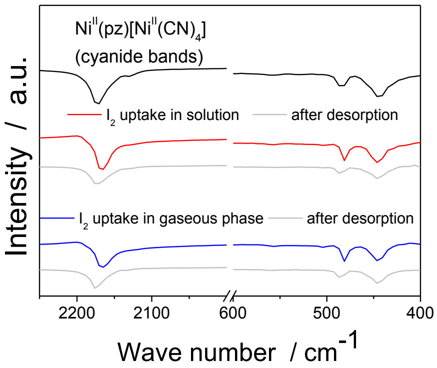
Ni^{II}(pz)[Ni^{II}(CN)$_4$]
(cyanide bands)
I$_2$ uptake in solution
after desorption
I$_2$ uptake in gaseous phase
after desorption
Intensity / a.u.
2200
2100
600
500
400
Wave number / cm^{-1}

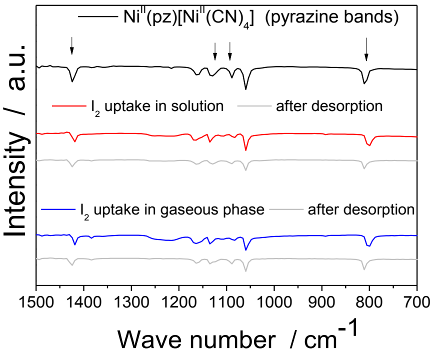
Ni^{II}(pz)[Ni^{II}(CN)$_4$] (pyrazine bands)
I$_2$ uptake in solution
after desorption
I$_2$ uptake in gaseous phase
after desorption
Intensity / a.u.
1500
1400
1300
1200
1100
1000
900
800
700
Wave number / cm^{-1}

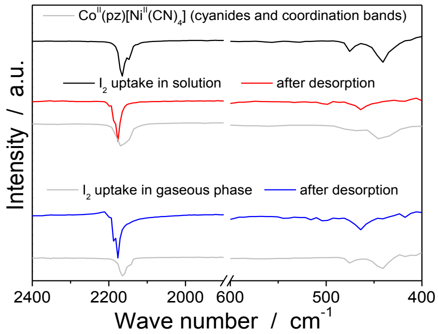
Co^{II}(pz)[Ni^{II}(CN)$_4$] (cyanides and coordination bands)
I$_2$ uptake in solution
after desorption
I$_2$ uptake in gaseous phase
after desorption
Intensity / a.u.
2400
2200
2000
600
500
400
Wave number / cm^{-1}

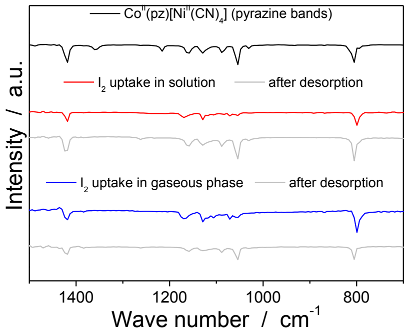
Co^{II}(pz)[Ni^{II}(CN)$_4$] (pyrazine bands)
I$_2$ uptake in solution
after desorption
I$_2$ uptake in gaseous phase
after desorption
Intensity / a.u.
1400
1200
1000
800
Wave number / cm^{-1}

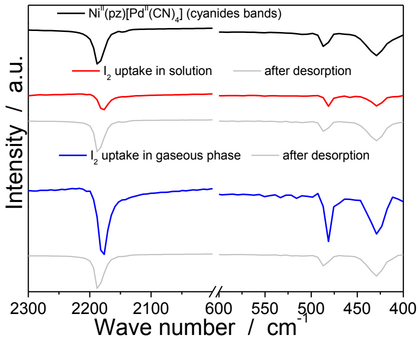
Ni^{II}(pz)[Pd^{II}(CN)$_4$] (cyanides bands)
I$_2$ uptake in solution
after desorption
I$_2$ uptake in gaseous phase
after desorption
Intensity / a.u.
2300
2200
2100
600
550
500
450
400
Wave number / cm^{-1}

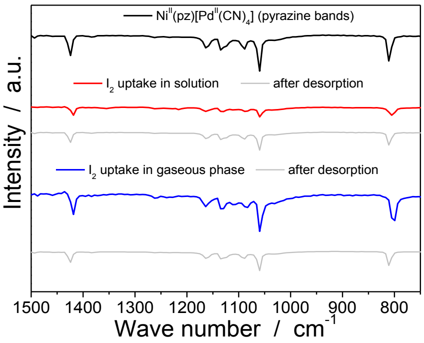
Ni^{II}(pz)[Pd^{II}(CN)$_4$] (pyrazine bands)
I$_2$ uptake in solution
after desorption
I$_2$ uptake in gaseous phase
after desorption
Intensity / a.u.
1500
1400
1300
1200
1100
1000
900
800
Wave number / cm^{-1}

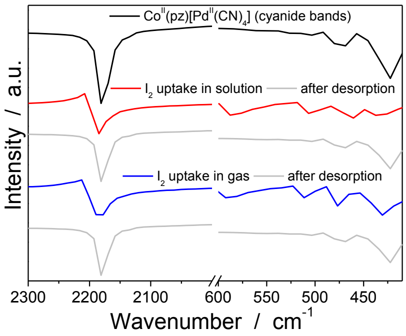
Co^{II}(pz)[Pd^{II}(CN)$_4$] (cyanide bands)
I$_2$ uptake in solution
after desorption
I$_2$ uptake in gas
after desorption
Intensity / a.u.
2300
2200
2100
600
550
500
450
Wavenumber / cm^{-1}

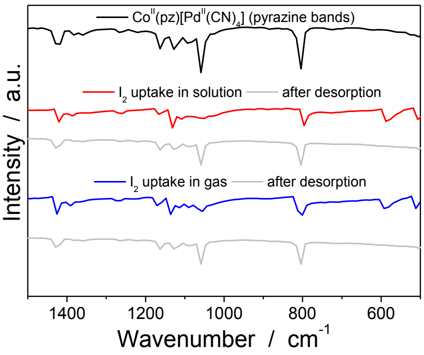
Co^{II}(pz)[Pd^{II}(CN)$_4$] (pyrazine bands)
I$_2$ uptake in solution
after desorption
I$_2$ uptake in gas
after desorption
Intensity / a.u.
1400
1200
1000
800
600
Wavenumber / cm^{-1}

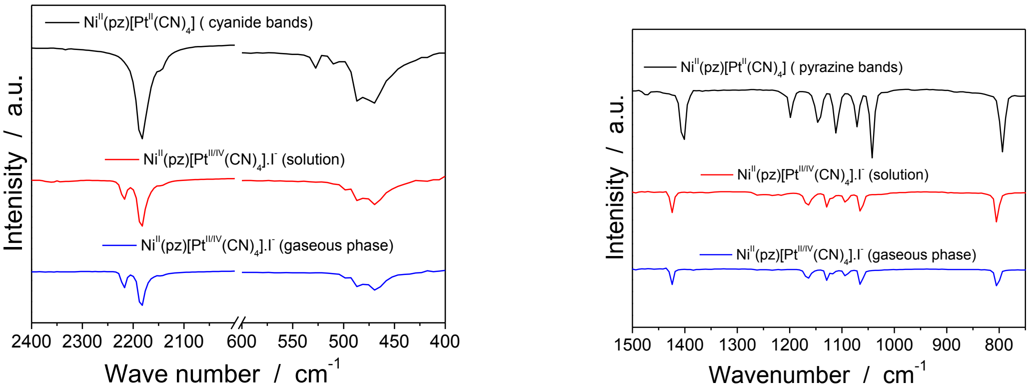

Fig. S2. FTIR spectra of M(pz)[M’(CN)$_4$]·2H$_2$O (M = Ni^{II}, Co^{II} and M’ = Ni^{II}, Pd^{II}, Pt^{II}, pz = pyrazine) before and after iodine loading. Note that the reference values for the pyrazine were measured experimentally from the related metal-pyrazine complexes.

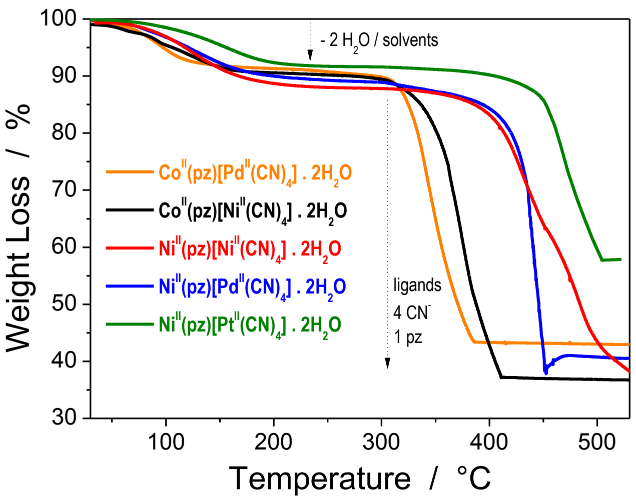

Fig. S3. Thermogravimetric analyses curves performed for a series of $M(pz)[M'(CN)_4]\cdot 2H_2O$ (M = Ni^{II}, Co^{II} and M' = Ni^{II}, Pd^{II}, Pt^{II}, pz = pyrazine). TGA curve inflexion points for the water removal: $Ni(pz)[Pt(CN)_4]\cdot 2H_2O$ T = 144 °C; $Ni(pz)[Pd(CN)_4]\cdot 2H_2O$ T = 121 °C; $Ni(pz)[Ni(CN)_4]\cdot 2H_2O$ T = 122 °C; $Co(pz)[Ni(CN)_4]\cdot 2H_2O$ T = 117 °C; $Co(pz)[Pd(CN)_4]\cdot 2H_2O$ T = 94 °C.

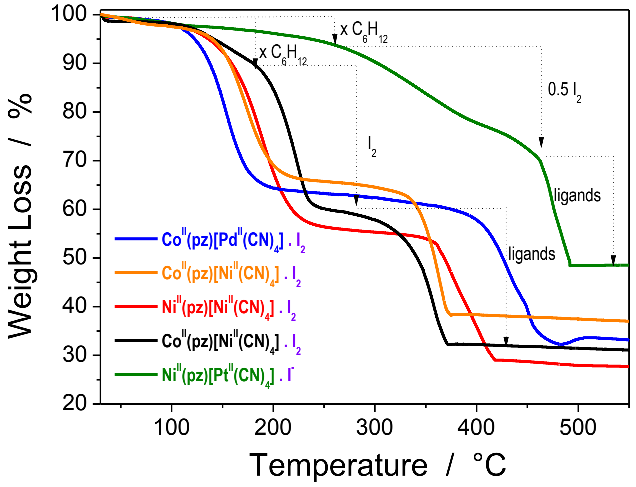

Fig. S4. Thermogravimetric analysis curves performed for a series of $M(pz)[M'(CN)_4]\cdot I_2$ (M = Ni^{II}, Co^{II} and M' = Ni^{II}, Pd^{II}, Pt^{II}, pz = pyrazine) and $Ni(pz)[Pt(CN)_4]\cdot I^-$ obtained by the iodine loading in cyclohexane solution.

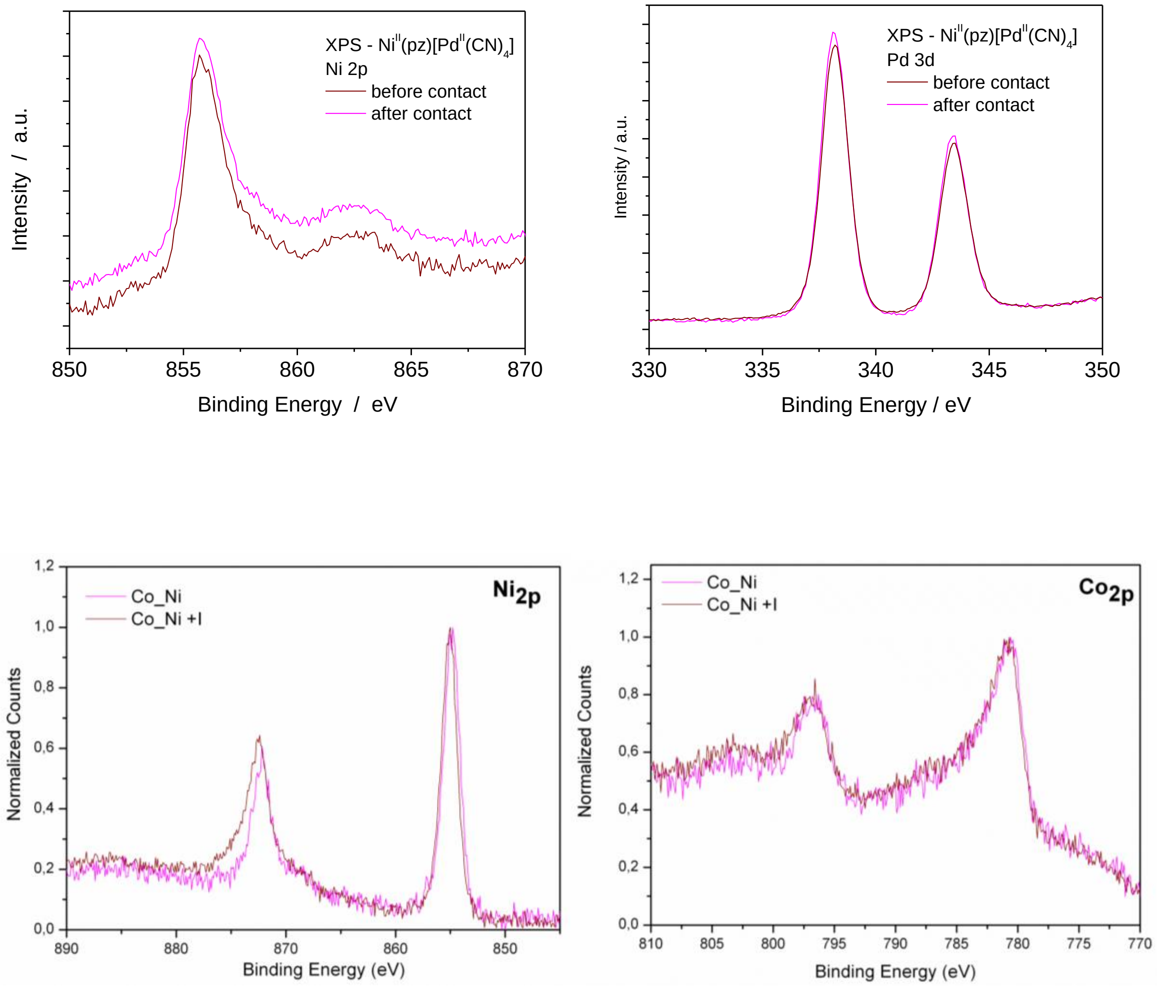

Fig. S5. XPS spectra for metallic centers in $Ni^{II}(pz)[Pd^{II}(CN)_4]$ and $Co^{II}(pz)Ni^{II}(CN)_4]$ before and after I_2 insertion in cyclohexane in the range of binding energy caracteristic of Ni 2p, Co 2p and Pd 3d orbitals.

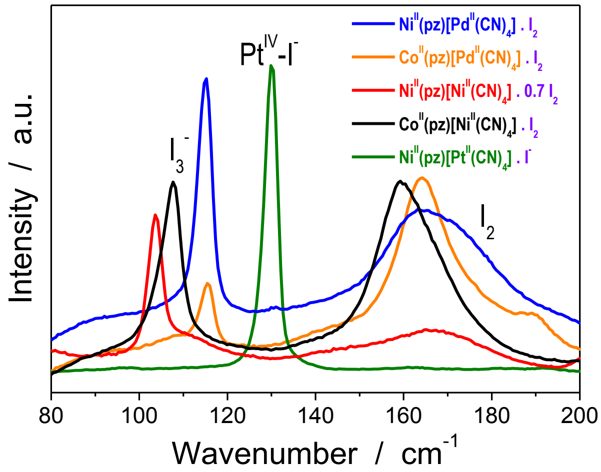

Fig. S6. Raman spectra for $M(pz)[M'(CN)_4]\cdot I_2$ (M = Ni^{II}, Co^{II} and M' = Ni^{II}, Pd^{II}, Pt^{II}, pz = pyrazine) and $Ni(pz)[Pt(CN)_4]\cdot 0.5I_2$ obtained by iodine loading in gas phase.

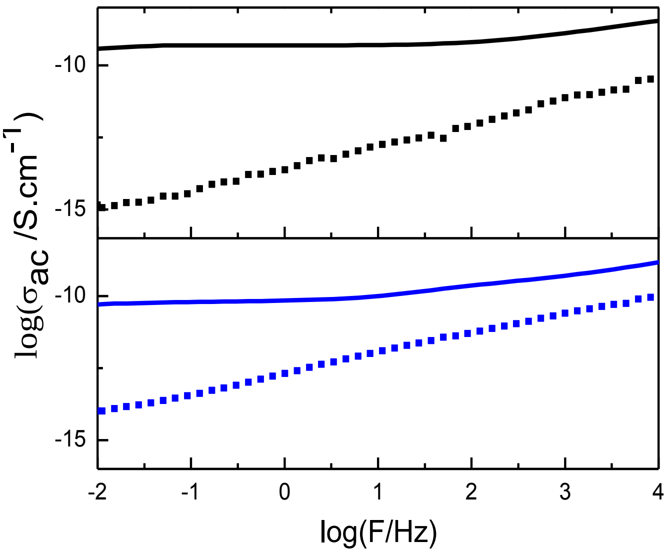

Fig. S7. Real part of the conductivity as a function of the frequency, recorded at 80°C for the empty (dashed line) and the iodine loaded (solid line) $Ni^{II}(pz)[Pd^{II}(CN)_4]$ (a) and $Co^{II}(pz)[Ni^{II}(CN)_4]$ (b).

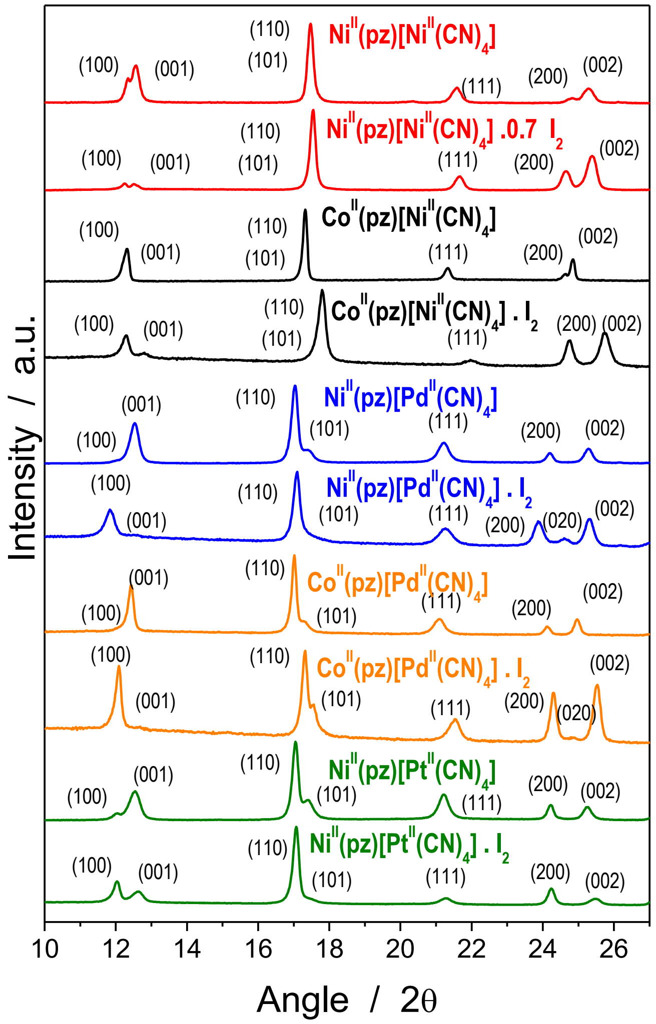

Fig. S8. X-Ray powder patterns for M(pz)[M'(CN)$_4$] (M^{II} = Ni^{II}, Co^{II} and M^{II}' = Ni^{II}, Pd^{II}, Pt^{II} and pz =pyrazine) before and after maximal iodine adsorption in gas phase.

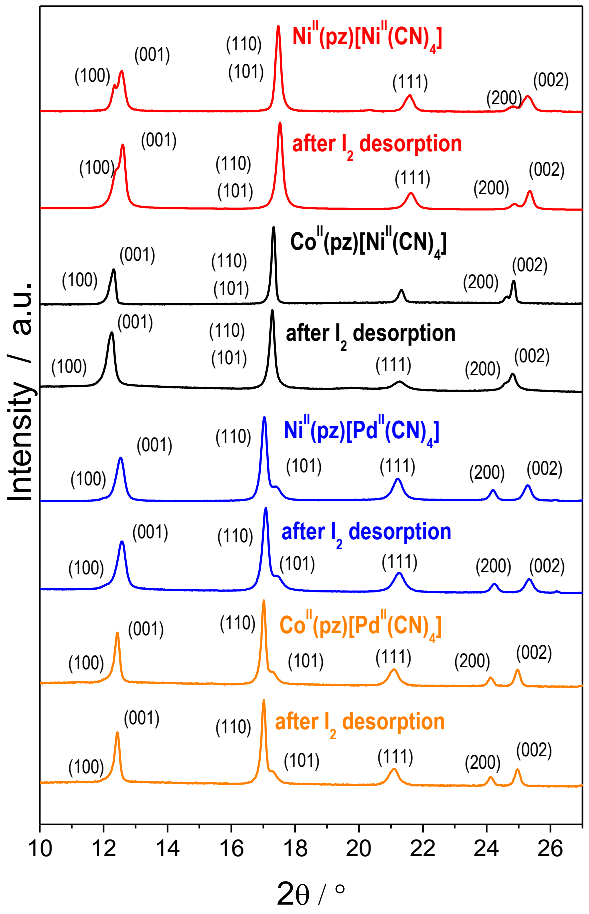

Fig. S9. X-Ray powder patterns for M(pz)[M'(CN)$_4$] (M^{II} = Ni^{II}, Co^{II} and M^{II}' = Ni^{II}, Pd^{II} and pz =pyrazine) after I$_2$ desorption (the iodine entrapment in solution).

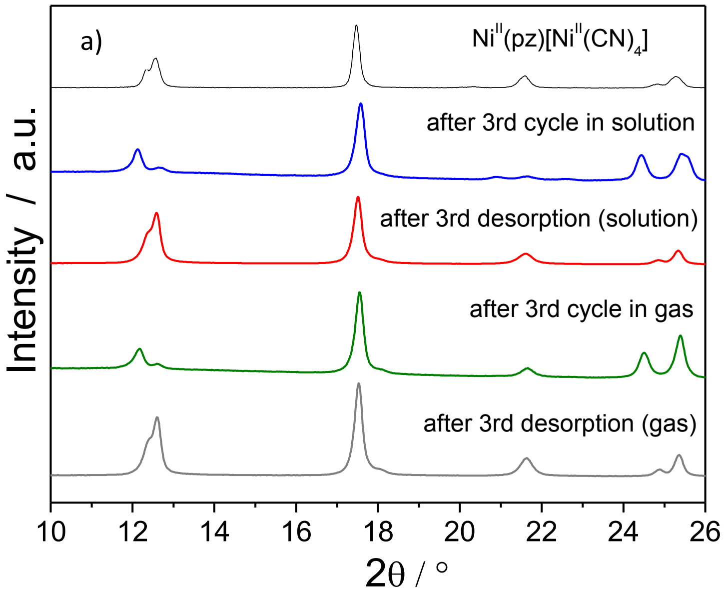

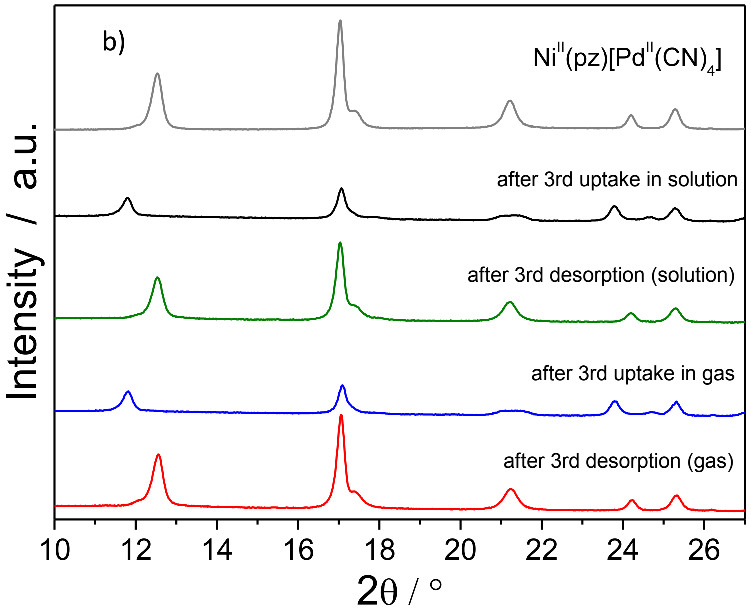

Fig. S10. X-Ray powder patterns for M(pz)[M’(CN)$_4$] (M^{II} = Ni^{II} and M$^{II’}$ = Ni^{II} (a), Pd^{II} (b) and pz =pyrazine) after 3 cycles of I$_2$ adsorption and desorption, in solution and in gas phase.

Selective entrapment of iodine in water vapours by the Hofmann-type structures.

Water is the most abundant species in the out-gases and it is important to investigate the iodine entrapment in the presence of water vapours. The iodine captures performed in gas already indicated that the $M^{II}(pz)[M^{II}(CN)_4]$ (M = Ni, Co, M' = Ni, Pd) clathrates maximal capacity is one I_2 molecule per unit cell. For $Ni^{II}(pz)[Ni^{II}(CN)_4]$, by contrast, the tests of entrapment in vapours only reached a capacity around $Ni^{II}(pz)[Ni^{II}(CN)_4]\cdot 0.8\ I_2$. It was assumed that a water steam could be physisorbed affecting the maximal capacity. In order to confirm this hypothesis, a new series of entrapments was performed for the host structures $Ni^{II}(pz)[Ni^{II}(CN)_4]$ and $Co^{II}(pz)[Ni^{II}(CN)_4]$. In hermetical containers, 100 mg of a dehydrated Hofmann-type structure and 800 mg of iodine were placed in separated open flasks and 10 ml of distilled water were added in the containers. The operating temperature was 80 °C and the tests were stopped after one week. Then the clathrates were dried in air and TGA curves, FT-IR and Raman spectra were registered. TGA curves after the I_2 entrapments in gas and in vapours of I_2 / H_2O for $Ni^{II}(pz)[Ni^{II}(CN)_4$ and $Co^{II}(pz)[Ni^{II}(CN)_4]$ are reported respectively in Fig. S11a - b.

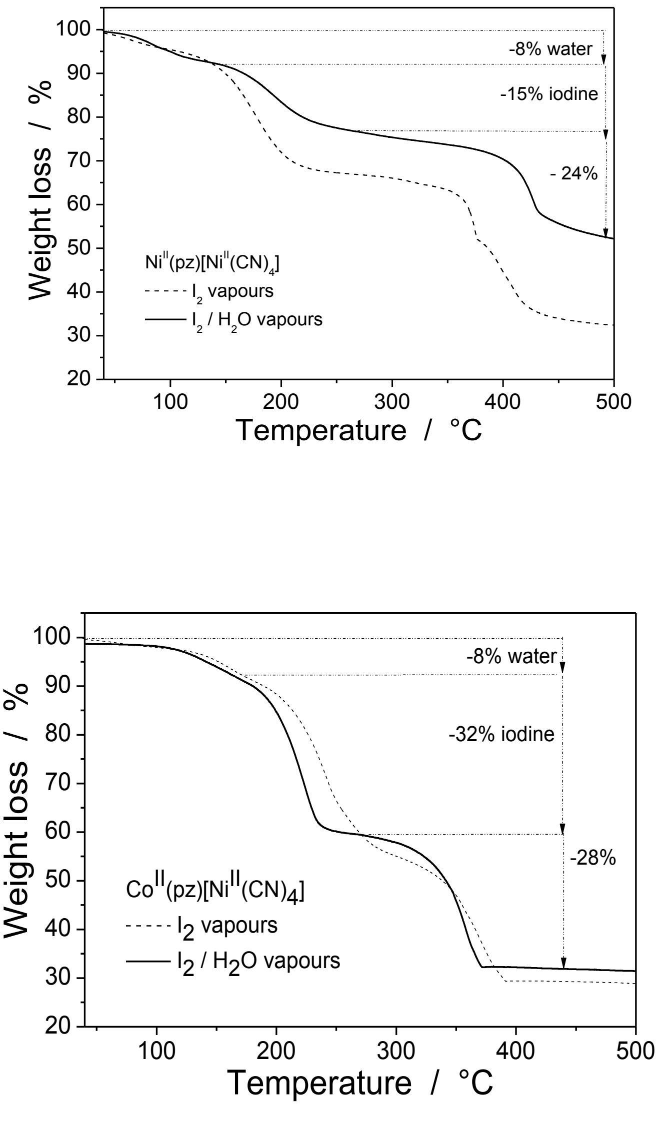

Fig. S11. TGA curves for the iodine loaded compound in the absence and in the presence of water vapors (selectivity test) with a) $Ni^{II}(pz)[Ni^{II}(CN)_4]$ and b) $Co^{II}(pz)[Ni^{II}(CN)_4]$.

Direct observations of TGA curves already suggest that the iodine entrapment with $Co^{II}(pz)[Ni^{II}(CN)_4]$ was not largely affected by the presence of water vapours, whereas a more significant reduction of the maximal capacity was clearly visible for nickel based structure. The entrapped iodine amounts in these conditions with the selected materials, were quantified by TGA (Table S1). In the case of $Ni^{II}(pz)[Ni^{II}(CN)_4]$, the detrimental effect of water was more important (37 %), while $Co^{II}(pz)[Ni^{II}(CN)_4]$ still showed a good capacity even though a decrease by 20% was observed. The nature of the confined iodine was verified by Raman spectroscopy. The spectra obtained after iodine capture by clathrates in I_2/H_2O vapours were compared to ones obtained for the capture of I_2 in gas, proving that the presence of water did not change the nature of the confined iodine.

Table S1. I_2 equivalents per unit cell after different conditions of entrapment**.**

Host structure	**C_6H_{12} solution**	**I_2 vapours**	**I_2/H_2O vapours**
$Ni^{II}(pz)[Ni^{II}(CN)_4]$	1 I_2	0.8 I_2	0.5 I_2
$Co^{II}(pz)[Ni^{II}(CN)_4]$	1 I_2	1 I_2	0.8 I_2

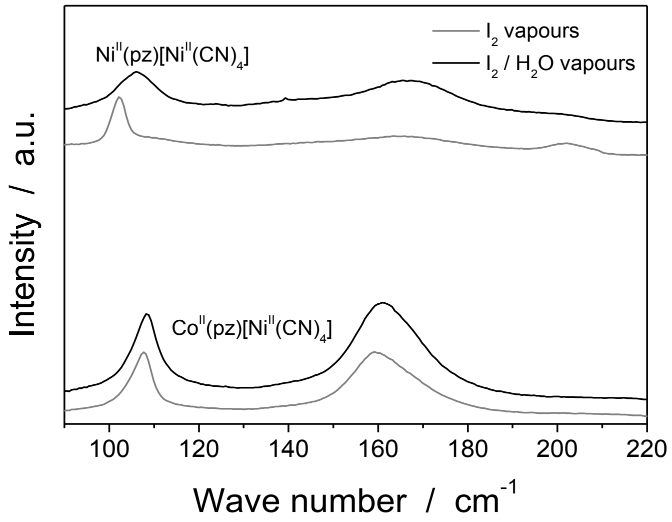

Fig. S12. Raman spectra for the investigated iodine loaded clathrates prepared in gaseous phase, with and without water steam.

The reason why the selectivity of $Co^{II}(pz)[Ni^{II}(CN)_4]$ was higher than the Ni-based analogue structure must be related to the different affinity of clathrates to water or to a *hydrophilicity* of the host structures. The *in-situ* FT-IR spectroscopy measurements were performed on the dehydrated structures $M(pz)[Ni^{II}(CN)_4]$, where M = Ni^{II} or Co^{II}, in order to evaluate how the change of the cation M could affect the affinity to water. The samples were prepared as thin tablets without diluting the products in any matrix. The tablets had to be fine enough to allow the recording of a transmission spectrum. We dehydrated the samples at 200 °C under primary vacuum inside a specific vacuum tube for FT-IR analyses. This tube consisted of a stopcock valve on one side, to branch to the vacuum line, and of an IR cell in KBr for the measurements on the other side. Then we recorded the spectra of the desorbed samples in the interval 3800-1500 cm^{-1} to check that no residual water remained after the thermal treatment. Subsequently, we closed the vacuum line and we sent through a different branch a small quantity of distilled water by controlling the pressure with an electronic barometer. When the pressure reached equilibrium after the adsorption of a small water quantity on the sample, a spectrum was recorded. This process was repeated up to an equilibrium pressure close to 18 mbar (saturation). Then, the pressure was gradually decreased by opening larger sections of the line. Finally the water was desorbed from the sample under primary vacuum for 1 hour, at room temperature. Spectra during the desorption process were registered as well. For a correct interpretation of the FT-IR spectra, a short remind of the FT-IR active band for the free H_2O and interacting H_2O is necessary. Since the shifts in IR-active bands for H_2O are related to the strength of the interaction with the Lewis acid (or base), this type of spectroscopic studies were largely exploited to investigate the surfaces of metal oxides and nanoporous aluminosilicates as zeolites.[1] The stretching mode ν(O-H) of free water is typically detected in higher region 3800-3700 cm^{-1} as a narrow band, but when water forms H-bonds with other oxygen of other H_2O molecules, typically another larger band appears due to Fermi resonance and it is located around 3400 cm^{-1} for the liquid state and around 3200 cm^{-1} for the tetrahedrally coordinated water.[2] The bending mode δ(O-H) of water is typically situated around 1600 cm^{-1}, with asymmetric shape, and it increases upon stronger H-bonding (for instance, 1630 cm^{-1} in liquid water). A decrease of δ(O-H) to 1580-1590 cm^{-1} can occur as well, for the coordinated water on a Lewis acid (*i.e.* metallic cations) where H_2O interacts through the lone pairs of the oxygens.

The spectra for the H_2O adsorption on $Ni^{II}(pz)[Ni^{II}(CN)_4]$ and $Co^{II}(pz)[Ni^{II}(CN)_4]$ in the bending region are reported in Fig. S13.

---

[1] a) Bordiga S., Regli L., Lamberti C., Zecchina A., Bjørgen M., *J. Phys. Chem. B* , 2005, **109**, 7724; b) Zecchina A., Coluccia S., Guglielminotti E., Ghiotti G. *The Journal of Physical Chemistry*, 1971, **76**, 18; c) Zecchina A., Coluccia S., Guglielminotti E., Ghiotti G., *J. Phys. Chem.*, 1971, **75**, 2774; d) Abramczyk H., Brozek-Pluska B., Surmacki J., Jablonska-Gajewicz J., Kordek R., *Journal of Biophysical Chemistry 2* 2011, 158.

[2] Paul J.B., Provencal R. A., Chapo C., Roth K., Casaes R., and Saykally R. J. *J. Phys. Chem. A*, 1999, **103**, 2972.

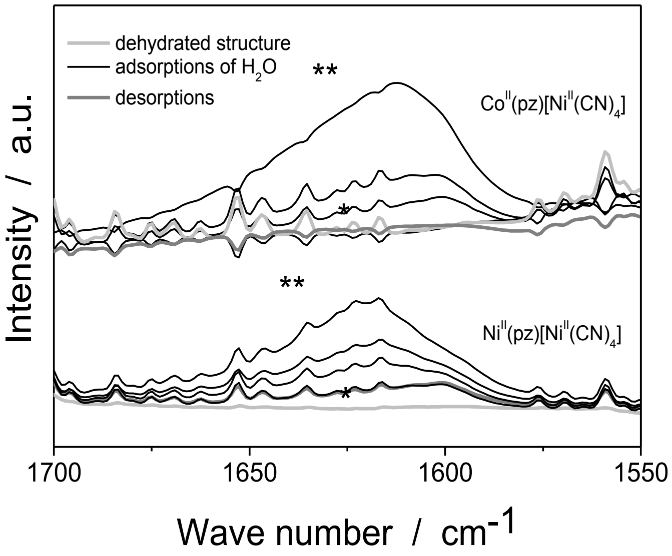

Fig. S13. Adsorptions of water on Hofmann-type structures in the bending region.

On both samples the first layer of adsorbed water showed a bending mode at 1598 cm^{-1} for Ni^{II}(pz)[Ni^{II}(CN)$_4$] and at 1601 cm^{-1} for Co^{II}(pz)[Ni^{II}(CN)$_4$] (Fig. S13b). These low values suggested that the first adsorbed water was coordinated on Lewis acid sites as Ni^{2+} and Co^{2+}. We could situate these sites on the surface of the samples where it was more probable to find metallic centres with non-saturated coordination sites. At higher pressures of water, the bending underwent a blue-shift to 1612 cm^{-1} for Co^{II}(pz)[Ni^{II}(CN)$_4$] and to 1620 cm^{-1} for Ni^{II}(pz)[Ni^{II}(CN)$_4$]. These values were still low for the typical bending mode of condensed water (1630 cm^{-1}) so that they suggested the formation of water clusters inside or outside the Hofmann-type structures. We could state that generally the value of δ(O-H) for the clusters is related to their dimensions: the bigger the cluster, the higher the δ(O-H) mode. For instance, measurements of the δ(O-H) mode for clusters $(H_2O)_n$ in gaseous phase reported in literature[3] indicated the following values: 1595 cm^{-1} for n = 1; 1600 cm^{-1} for n = 2; 1610 cm^{-1} for n = 3; 1630 cm^{-1} for n = 4. Bending modes at high pressures on both Hofmann-type structures were very large with a more symmetric shape for Ni^{II}(pz)[Ni^{II}(CN)$_4$], so that clusters of different size had to be present on both samples. However, the higher δ(O-H) mode on Ni^{II}(pz)[Ni^{II}(CN)$_4$] suggested a larger amount of bigger clusters. On desorption at room temperature a relevant difference between the two samples was detected. Gradual decrease of water pressure immediately desorbed all the water off the Co^{II}(pz)[Ni^{II}(CN)$_4$] sample and after one hour under primary vacuum no δ(O-H) mode was visible anymore. By contrast, after one hour of primary vacuum on Ni^{II}(pz)[Ni^{II}(CN)$_4$], the δ(O-H) mode for water clusters disappeared but the band at 1598 cm^{-1} related to the coordinated water on Lewis acid sites Ni^{2+} was still visible.

Thus, data indicated the formation of more stable complexes with water on the surface of Ni^{II}(pz)[Ni^{II}(CN)$_4$]. On the other side, the complexes formed on the surface of Co^{II}(pz)[Ni^{II}(CN)$_4$] were easily destabilized and destroyed by reducing the pressure at room temperature. These data correlated with the experimental observations about the rehydration process of the two materials: when the dehydrated Ni^{II}(pz)[Ni^{II}(CN)$_4$] (grey powder) was exposed to air, it rapidly adsorbed water molecules on the surface, exhibiting again the violet colour of the hydrated structure. By contrast, the dehydrated Co^{II}(pz)[Ni^{II}(CN)$_4$] (blue powder) recovered very slowly the pink colouration of the hydrated structure. We could expect that the rehydration may be partially due to the water sorption inside the cages.

This higher affinity on Ni^{2+} sites maybe then correlated with the higher decrease in iodine loading capacity during the entrapment of I_2 in water vapours. We can finally formulate the hypothesis that when unsaturated Ni^{2+} cations were present on the grain surface, stable water complexes formed rapidly and the diffusion of I_2 was partially hindered by water since the molecular I_2 and H_2O have opposite polarities. Hence, the structure Co^{II}(pz)[Ni^{II}(CN)$_4$] exhibited a better selectivity due to formation of less stable complexes with water.

POWDER X-RAY DIFFRACTION LEBAIL REFINEMENTS.

The diffraction patterns of the crystalline phases Ni^{II}(pz)[Ni^{II}(CN)$_4$] and analogues were measured at room temperature in the glass capillary configuration on the two circle Panalytical XPERTPro diffractometer mounted in a Debye-Sherrer configuration and equipped with a Cu K$_{alpha}$ radiation. For the iodine clathrate Ni^{II}(pz)[Ni^{II}(CN)$_4$]@I_2 and analogues a planar configuration with rotating diffraction angle was preferred due to difficulties in the capillary preparation. The samples in this configuration were analyzed with a long exposure of 12 hours (1000 s on each step with interval 0.16°). The nature of the

---

[3] Paul J.B., Provencal R. A., Chapo C., Roth K., Casaes R., and Saykally R. J. *J. Phys. Chem. A*, 1999, **103**, 2972.

crystalline phase was confirmed by indexing the whole diffraction pattern, a whole-pattern decomposition (Lebail fitting) with constant scale factor and a Pseudo-Voigt function profil was then applied using Fox software.[4] LeBail refinement techniques using Fullproff software[5] were used in order to perform a profile refinement of diffraction peaks. The scale factor, zero point of detector, background parameters and lattice constants were refined in the first round, then peak shape and asymmetry parameters were then added when the models had already converged. Finally, instrumental or physical aberration corrections were added to the least squares refinement by using parameters sycos and sysin. Results of refinement are given below as supplementary information.

Refinement for $Ni^{II}(pz)[Ni^{II}(CN)_4]$

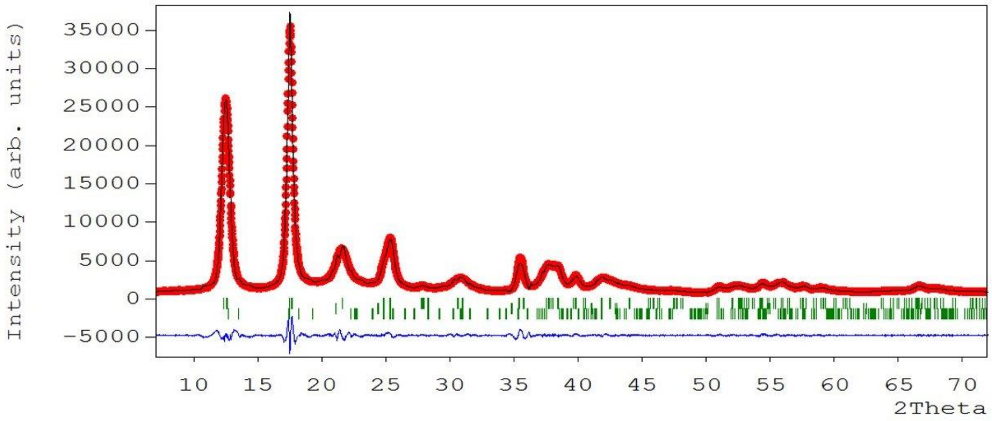

Fig. S14. Tetragonal system; Space group *P4/m*. Cell Parameters: $a = b = 7.1762(3)$ Å, $c = 7.0316(5)$ Å, $\alpha = \beta = \gamma = 90.0°$, Vol: 362.10(3) Å^3.

---

[4] J. Appl. Cryst., 2002, 35, 734-743, V. Favre-Nicolin and R. Cermy, Fox, 'Free objects for crystallography': a modular approach to ab initio structure determination from powder diffraction.

[5] Fullprof 2000 version July 2001, Juan Rodrigues-Carvajal, Laboratoire Leon Brillouin (CEA-CNRS), 91191 Gif sur Yvette Cedex, France.

Refinement for $Ni^{II}(pz)[Ni^{II}(CN)_4]\cdot I_2$

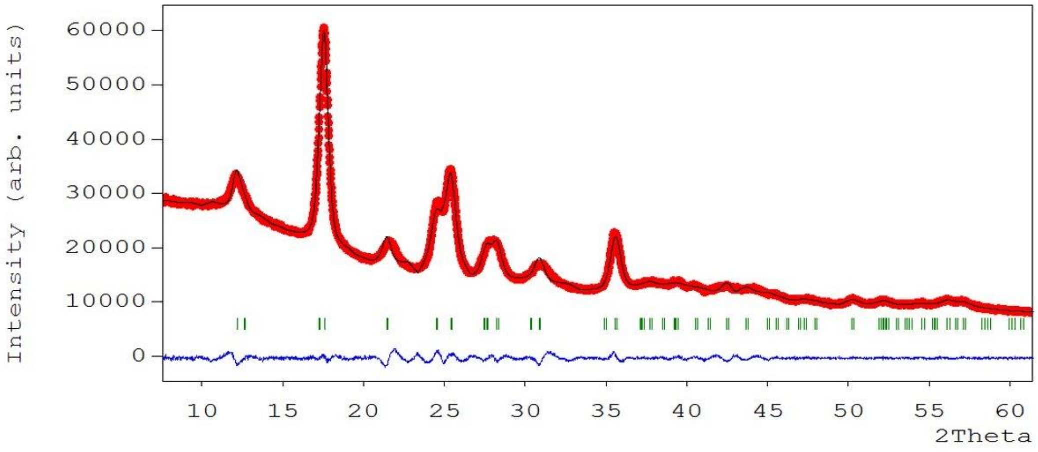

Fig. S15. Tetragonal system; Space group *P4/m*. Cell parameters: $a = b = 7.2605(6)$ Å, $c = 7.0072(5)$ Å, $\alpha = \beta = \gamma = 90.0°$, Vol: 369.385(2) $Å^3$.

Refinement for $Ni^{II}(pz)[Pd^{II}(CN)_4]$

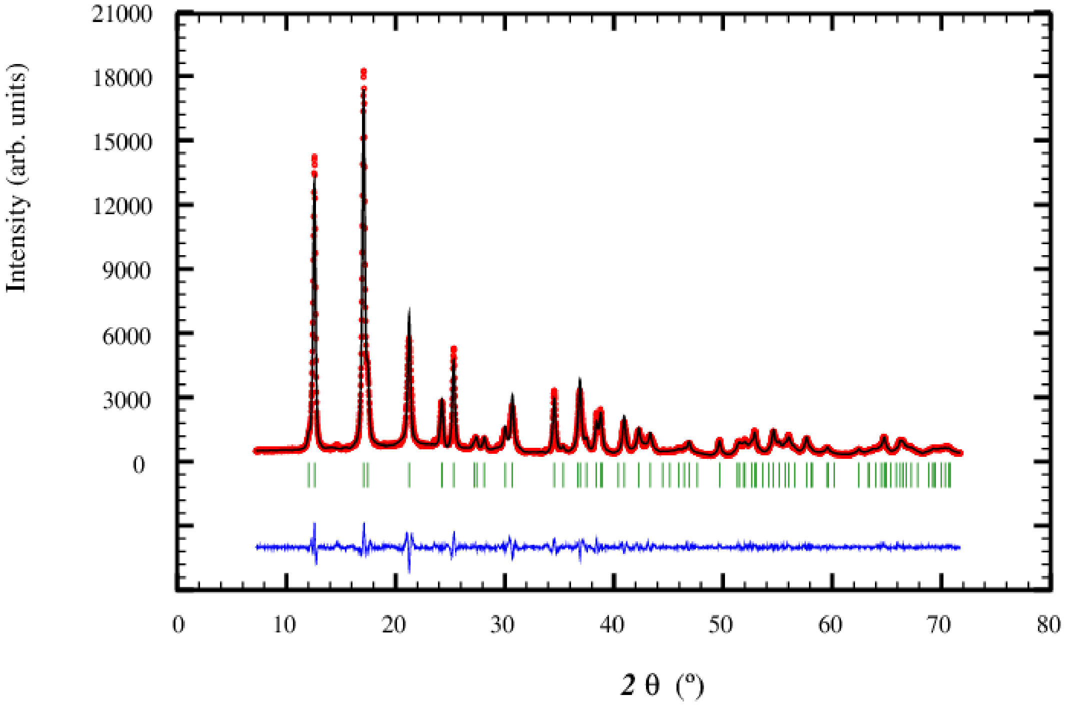

Fig. S16. Tetragonal system; Space group P4/m. *Cell parameters: $a = b = 7.3334(3)$ Å, $c = 7.0253(4)$ Å $\alpha = \beta = \gamma = 90.0°$ Vol: 377.81(3)* $Å^3$.

Refinement for Ni^{II}(pz)[Pd^{II}(CN)$_4$]·I$_2$

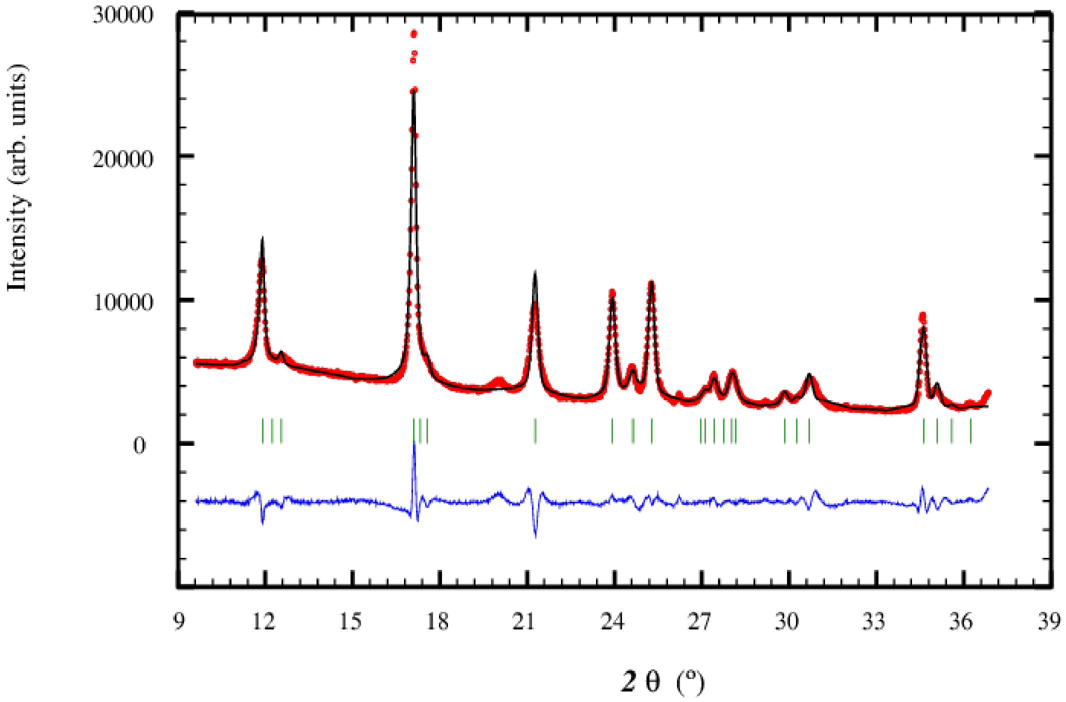

Fig. S17. *Orthorhombic system; Space group Pmmm. Cell parameters: a = 7.431(1) Å, b = 7 .223(1) Å, c = 7 .0395(8) Å α = β = γ = 90.0°. Vol: 377.82(9)* Å^3.

Refinement for Ni^{II}(pz)[Pt^{II}(CN)$_4$]

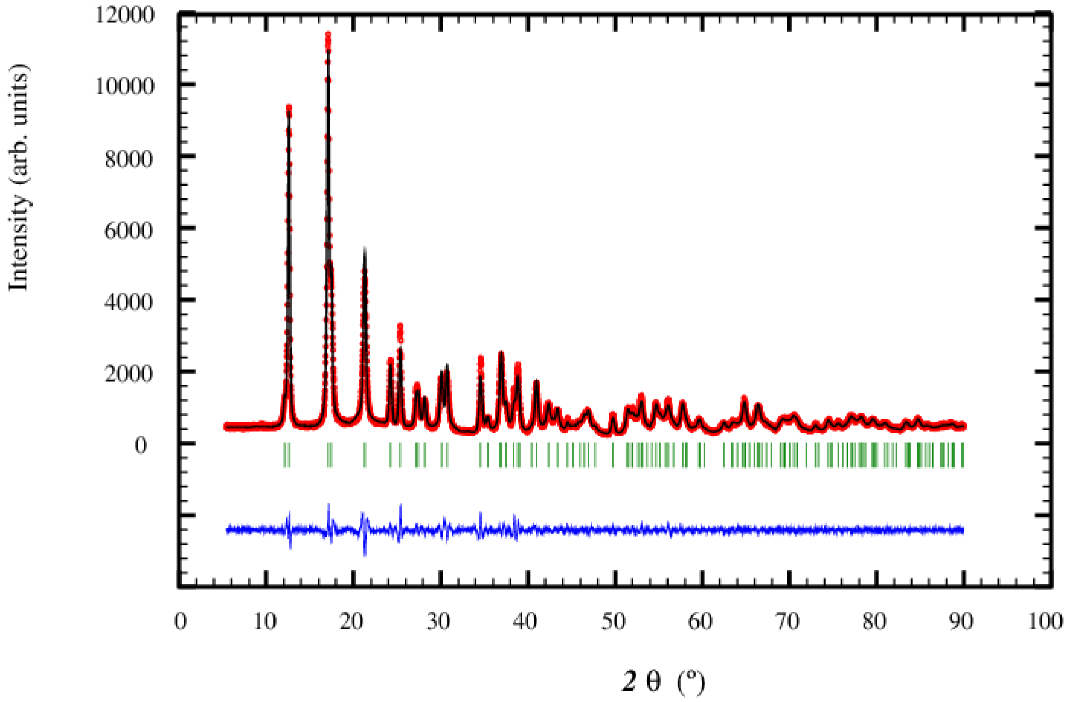

Fig. S18. Tetragonal system; Space group *P*4/*m*, cell parameters: Cell parameters: *a* = *b* = *7.3244(3)* Å, *c* = *7.0239(4)* Å *α* = *β* = *γ* = *90.0°*, Vol: 376.81(3) Å^3.

Refinement for $Ni^{II}(pz)[Pt^{II/IV}(CN)_4]\cdot I^-$

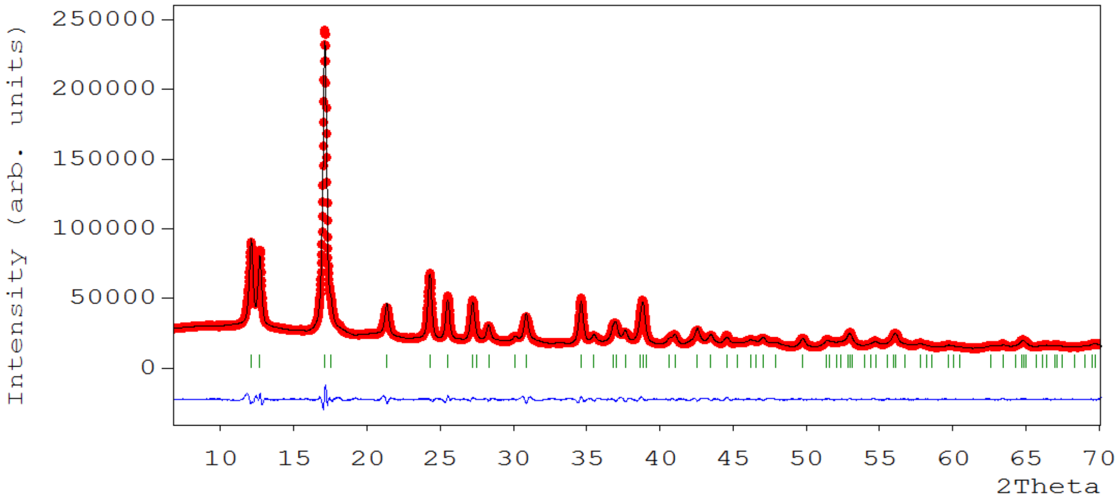

Fig. S19. Tetragonal system; Space group P 4/m. Cell parameters: $a = b = 7.1775(3)$ Å, $c = 6.9789(4)$ Å $\alpha = \beta = \gamma = 90.0°$, Vol: 359.53(3) Å^3.

Refinement for $Co^{II}(pz)[Ni^{II}(CN)_4]$

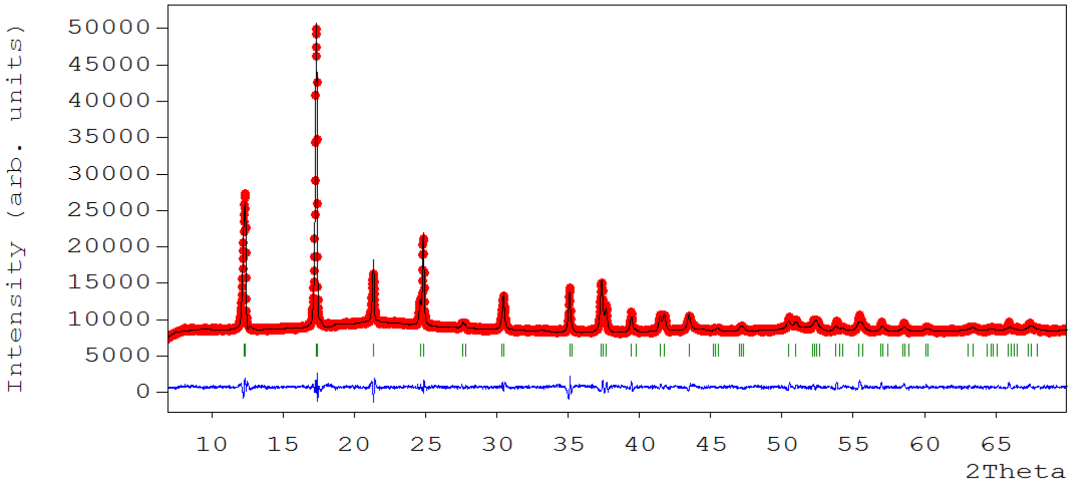

Fig. S20. Tetragonal system; Space group P 4/m. Cell parameters: $a = b = 7.2262(7)$ Å, $c = 7.1594(9)$ Å, $\alpha = \beta = \gamma = 90.0°$, Vol: 373.84(9) Å^3.

Refinement for Co^{II}(pz)[Ni^{II}(CN)$_4$]·I$_2$

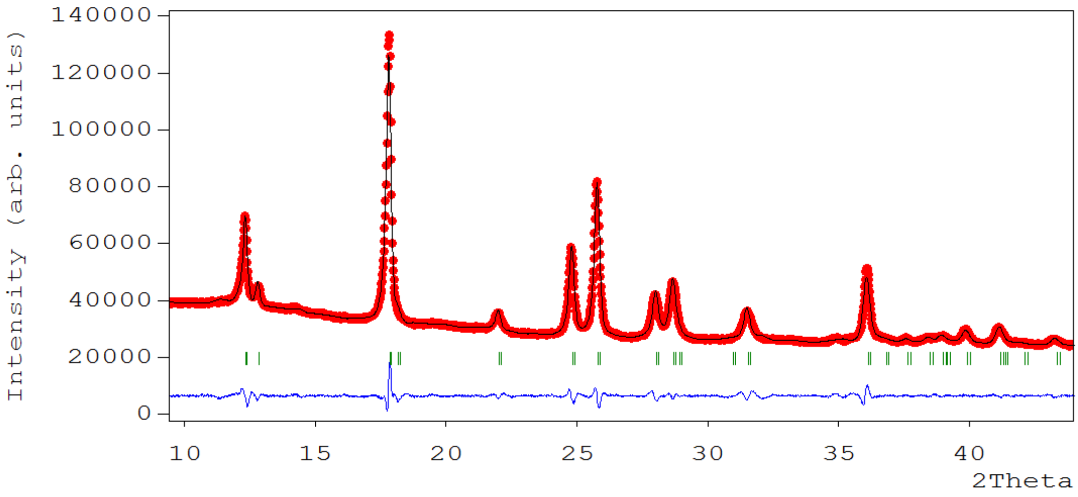

Fig. S21. Tetragonal system; Space group P 4/m, Cell parameters: *a* = *b* = 7.1593(5) Å, *c* = 6.8942(5) Å, $\alpha = \beta = \gamma = 90.0°$, Vol: 353.3(6) Å^3.

Refinement for Co^{II}(pz)[Pd^{II}(CN)$_4$]

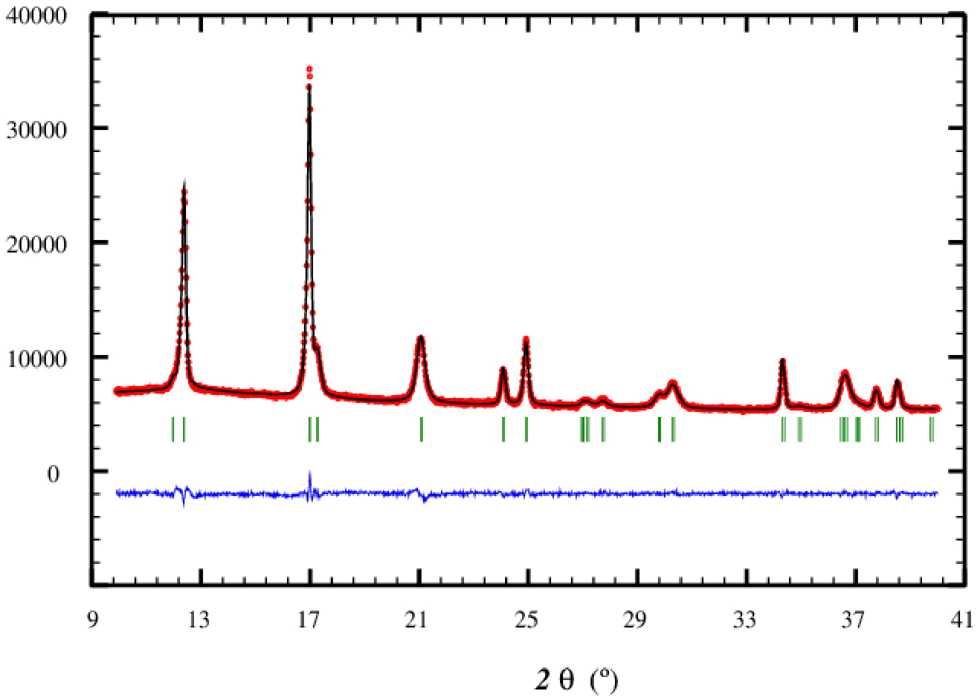

Fig. S22. Tetragonal system; Space group *P4/m.* Cell parameters: *a* = *b* = 7.3865(3) Å, *c* = 7.1446(4) Å, $\alpha = \beta = \gamma = 90.0°$, Vol: 398.82(3) Å^3.

Refinement for $Co^{II}(pz)[Pd^{II}(CN)_4]\cdot I_2$

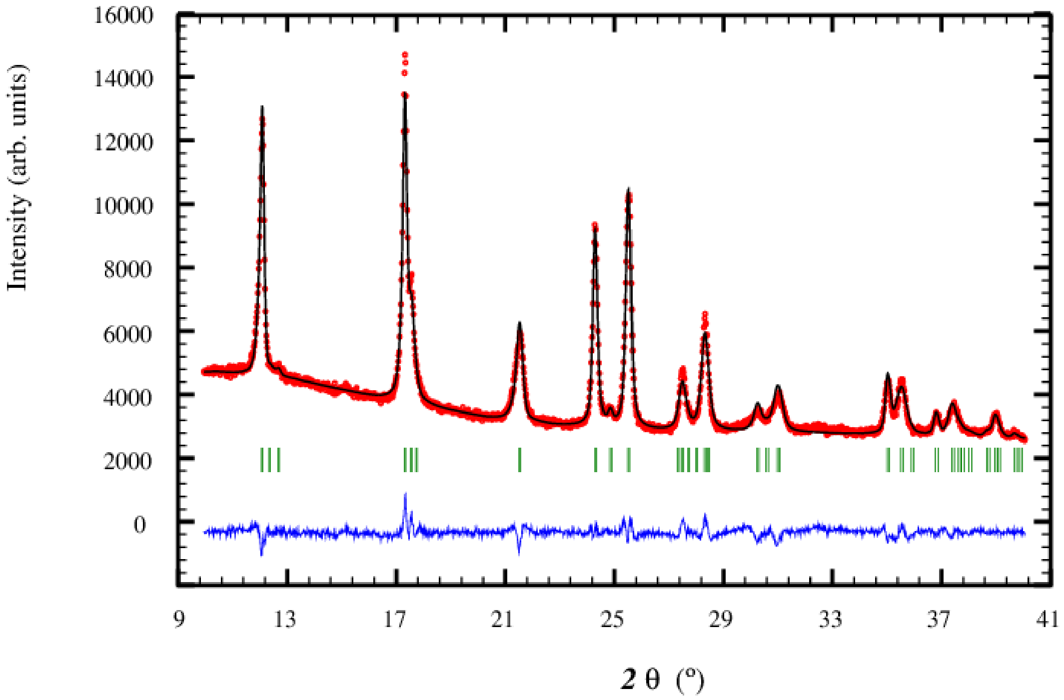

Fig. S23. Orthorhombic system; Space group *Pmmm*. Cell parameters: a = 7.3229(6) b =7.1627(8) Å, c = 6.9786(5) Å, $\alpha = \beta = \gamma = 90.0°$, Vol: 366.05(5) $Å^3$.